POLITECNICO DI TORINO
Repository ISTITUZIONALE

An MBSE Framework for the Feasibility Assessment of a Modular Planetary Sunshade System

Original
An MBSE Framework for the Feasibility Assessment of a Modular Planetary Sunshade System / Coco, M., Chesley, B., Romano, M., Cappelletti, C.. - In: ACTA ASTRONAUTICA. - ISSN 1879-2030. - 251:(2027), pp. 584-595. [10.1016/j.actaastro.2026.10.027]

Availability:
This version is available at: 11583/3015615 since: 2026-10-28T10:58:03Z

Publisher:
Elsevier

Published
DOI:10.1016/j.actaastro.2026.10.027

Terms of use:

This article is made available under terms and conditions as specified in the corresponding bibliographic description in the repository

Publisher copyright

(Article begins on next page)

31 October 2026

Acta Astronautica 251 (2027) 584–595

Contents lists available at ScienceDirect

Acta Astronautica

journal homepage: www.elsevier.com/locate/actaastro

An MBSE framework for the feasibility assessment of a modular Planetary Sunshade System ☆

Marina Coco [a,*], Bruce Chesley [b], Marcello Romano [c], Chantal Cappelletti [d]

[a] Department of Mechanical and Aerospace Engineering, Politecnico di Torino, Corso Duca degli Abruzzi, 24, Turin, 10129, Italy
[b] Teaching Science and Technology, Inc., Monument, CO, 719-494-9739, USA
[c] Chair of Astrodynamics, Technical University of Munich, Willy-Messerschmitt-Str. 11, Munich, 82024, Germany
[d] Department of Mechanical, Materials and Manufacturing Engineering, University of Nottingham, Nottingham, NG7 2RD, United Kingdom

ARTICLE INFO

Keywords:
Planetary Sunshade System
Space-based solar geoengineering
Model-Based Systems Engineering
Feasibility assessment

ABSTRACT

The feasibility of a Planetary Sunshade System (PSS) strongly depends on architectural choices, system scalability, and controllability, among other critical challenges. Modular architectures offer potential advantages in terms of manufacturing, deployment, system robustness, and reversibility, while introducing significant challenges related to system integration and control complexity. This paper presents a Model-Based Systems Engineering (MBSE) framework for a traceable and parametric feasibility assessment of a modular PSS architecture. The framework links mission needs and objectives, functional analysis, high-level requirements, configuration-specific requirements, parametric sizing, and quantitative feasibility measures within an updateable engineering structure. The approach is applied to a representative precursor demonstrator configuration to show how system-level assumptions can be progressively connected to preliminary subsystem sizing and feasibility metrics throughout an iterative process. The application case includes the definition of a reference mission and configuration, preliminary sizing, required attitude and orbital control system torque evaluation, actuator feasibility assessment, subsystem selection, and preliminary mass, power, and communication budgets. Derived requirements are then connected to the corresponding sizing and analysis artifacts to support requirements traceability and future design iterations. The results provide a first quantitative feasibility assessment of the precursor demonstrator within the adopted assumptions. They indicate that the proposed framework can support the transition from high-level PSS concepts to configuration-level technical assessments, while identifying critical aspects to be refined in future mission studies and digital-twin-oriented developments.

1. Introduction

Solar geoengineering concepts have been proposed as possible approaches to help mitigate anthropogenic climate change by reducing a fraction of the incoming solar radiation reaching Earth. These approaches are not intended to replace emission reduction and adaptation strategies, but they have been investigated as potential complementary options to limit global temperature increase.

Among the proposed Solar Radiation Management (SRM) concepts, space-based solar geoengineering has received renewed attention. In this context, a Planetary Sunshade System (PSS) would consist of a large-scale space-based architecture designed to reduce the incoming solar radiation reaching Earth. One possible implementation relies on a swarm of solar-sail spacecraft operating near the displaced photo-gravitational equilibrium point L_1^* of the Sun–Earth/Moon Center of Mass (CoM) system, thereby partially casting a shadow on Earth.

However, achieving a climate-relevant shading effect would require an unprecedented space-engineering effort. The required equivalent shading area, the number of spacecraft, the deployment and maintenance strategy, and the long-term controllability of the architecture make the direct implementation of a full-scale PSS unrealistic without a progressive development path.

Previous studies have investigated sunshade concepts from different perspectives, including early concepts for space-based solar radiation reduction, clouds of small spacecraft near the Sun–Earth L_1 point, optimal sunshade configurations, trajectory optimization, and photo-gravitational equilibrium orbits for planetary sunshade missions [1–5].

☆ This article is part of a Special issue entitled: 'Planetary Sunshade' published in Acta Astronautica.

* Corresponding author.
E-mail addresses: marina.coco@polito.it (M. Coco), bruce.c.chesley@gmail.com (B. Chesley), marcello.romano@tum.de (M. Romano), Chantal.Cappelletti@nottingham.ac.uk (C. Cappelletti).

https://doi.org/10.1016/j.actaastro.2026.10.027
Received 14 June 2026; Received in revised form 1 October 2026; Accepted 14 October 2026
Available online 21 October 2026
0094-5765/© 2026 The Authors. Published by Elsevier Ltd on behalf of IAA. This is an open access article under the CC BY license (http://creativecommons.org/licenses/by/4.0/).

More recent work has further addressed practical feasibility assessments of sunshade systems, transparent occulters, modular and deployable architectures, technology roadmaps, precursor mission concepts, performance of solar-sail materials at L_1^*, and integrated MBSE/MBE-based system analysis as intermediate steps toward a long-term PSS architecture [6–12]. However, the application of a structured systems-engineering process to PSS development remains at an early stage. A systematic framework is therefore needed to support the traceable transition from high-level concepts to quantitative technical feasibility assessments, while establishing the basis for future updateable digital-twin representations of the system.

This paper introduces an MBSE Digital Twin-oriented framework for the traceable and parametric feasibility assessment of a modular PSS and applies it to a representative demonstrator configuration. The framework links PSS mission needs and objectives, functional analysis, and high-level requirements to configuration-specific requirements, parametric sizing, and quantitative feasibility measures. In this way, high-level mission objectives can be progressively translated into assessable engineering quantities and subsystem-level design constraints. Derived requirements and feasibility outputs can then be connected to support an initial feasibility assessment and future design iterations.

The remainder of the paper is organized as follows. Section 2 introduces the modular PSS concept and reference architecture. Section 3 describes the MBSE framework and the parametric sizing methodology. Section 4 applies the framework to a first precursor demonstrator and presents the corresponding preliminary feasibility assessment. Finally, Section 5 discusses conclusions and future work.

2. Modular PSS concept and reference architecture

The Planetary Sunshade System (PSS) considered in this work is based on a modular and distributed architecture. A modular approach is adopted to support scalability, progressive deployment, redundancy, replacement, and potential reversibility.

A technology development roadmap for a PSS has been developed in previous work [9]. In the present work, that roadmap is used as background to define the reference modular architecture and the configuration families considered in the proposed feasibility framework. The purpose of this section is therefore to establish the architectural context required for the traceable framework developed in the following sections.

The main architecture drivers are briefly discussed here. The first driver is the climate objective, commonly expressed as a required solar-insolation reduction. In this work, a reduction of approximately 1.7% is considered, consistently with previous studies [13]. This corresponds to an equivalent shaded area of approximately 6.5×10^6 km^2. This scale motivates the adoption of a distributed swarm architecture rather than a monolithic structure. The distributed approach is also motivated by safety, scalability, redundancy, potential reversibility, and the need for a high degree of operational autonomy. A multi-cluster architecture may further improve redundancy, scalability, and shadowing efficiency, while preserving safety distances between spacecraft.

Communication and navigation also drive the reference architecture. Because of the expected number of individual spacecraft, direct communication between every sunshade unit and Earth would not be practical for a full-scale distributed system. Therefore, the reference architecture adopts a hierarchical communication and coordination logic [14]. Inter-satellite links (ISL) and radio-ranging capabilities are considered to support relative navigation, data exchange, and reduced dependence on continuous ground support.

These considerations lead to a functional differentiation between swarm elements and higher-level coordination or relay elements. In the target architecture, swarm elements contribute to the overall solar-shading function and communicate primarily with other swarm elements or relay nodes. Higher-level coordination or relay elements support distributed operations, data aggregation, and communication with the Ground Segment.

This architectural logic provides the basis for the configuration families introduced in the following subsections and for the MBSE framework developed in Section 3.

2.1. Target modular architecture

The target full-scale architecture is conceived as a distributed swarm of modular sunshade units supported by higher-level coordination and communication elements. It includes two main space-segment elements: the Baseline Module (BM) and the Mothership Module (MM). The Ground Segment is retained as the supporting mission-operations element.

The BM represents the repeatable building block of the modular PSS architecture. In a full-scale architecture, a large number of BM units would operate as the distributed swarm and would be coordinated to provide the required equivalent shaded area. The BM is assumed to communicate primarily through inter-satellite links, either with other BMs or with higher-level coordination elements.

The MM is introduced as a higher-level coordination and relay element. Its role is to support distributed operations, enable communication between different levels of the system, aggregate data from the swarm, and provide relay capability toward the Ground Segment. The Ground Segment supports command, monitoring, mission planning, and data-processing activities.

The PSS development roadmap also includes precursor missions, intended to demonstrate key enabling technologies before the implementation of the full-scale system. This introduces a distinction between the target PSS architecture and precursor mission configurations. Precursor spacecraft may include capabilities that are useful for demonstration and validation, but are not necessarily representative of every unit in the final full-scale swarm.

2.2. Reference configuration families

To connect the full-scale architecture with a progressive development path, four reference configuration families are considered: Prototype 1 (P1), Prototype 2 (P2), the BM, and the MM. P1 and P2 represent precursor mission configurations, while the BM and the MM represent target full-scale architecture elements. These configurations do not represent the same level of maturity or design detail. Instead, they correspond to different roles within the development of the modular PSS concept, from early precursor demonstration to full-scale distributed operations.

P1 is defined as an early precursor demonstrator. Its purpose is to provide a first implementation of selected functions and technologies relevant to the PSS. P1 is therefore not intended to represent the final PSS module, but rather the first configuration-specific application case for the feasibility framework.

P2 is considered as a larger-scale demonstrator intended to extend the precursor logic toward more representative dimensions, communication strategies, and operational capabilities.

The BM and MM correspond to the target full-scale architecture elements introduced before: the BM as the repeatable swarm element, and the MM as the coordination and relay element supporting distributed operations.

A key distinction between these configuration families concerns their communication capability. P1 intentionally includes direct Earth communication because it is a precursor demonstrator. P2 extends this logic by combining inter-satellite links with Earth communication. In contrast, the BM is assumed to rely primarily on inter-satellite links, while Earth communication and coordination functions are delegated to MM and to the Ground Segment. This distinction reflects the hierarchical communication logic adopted for the full-scale architecture.

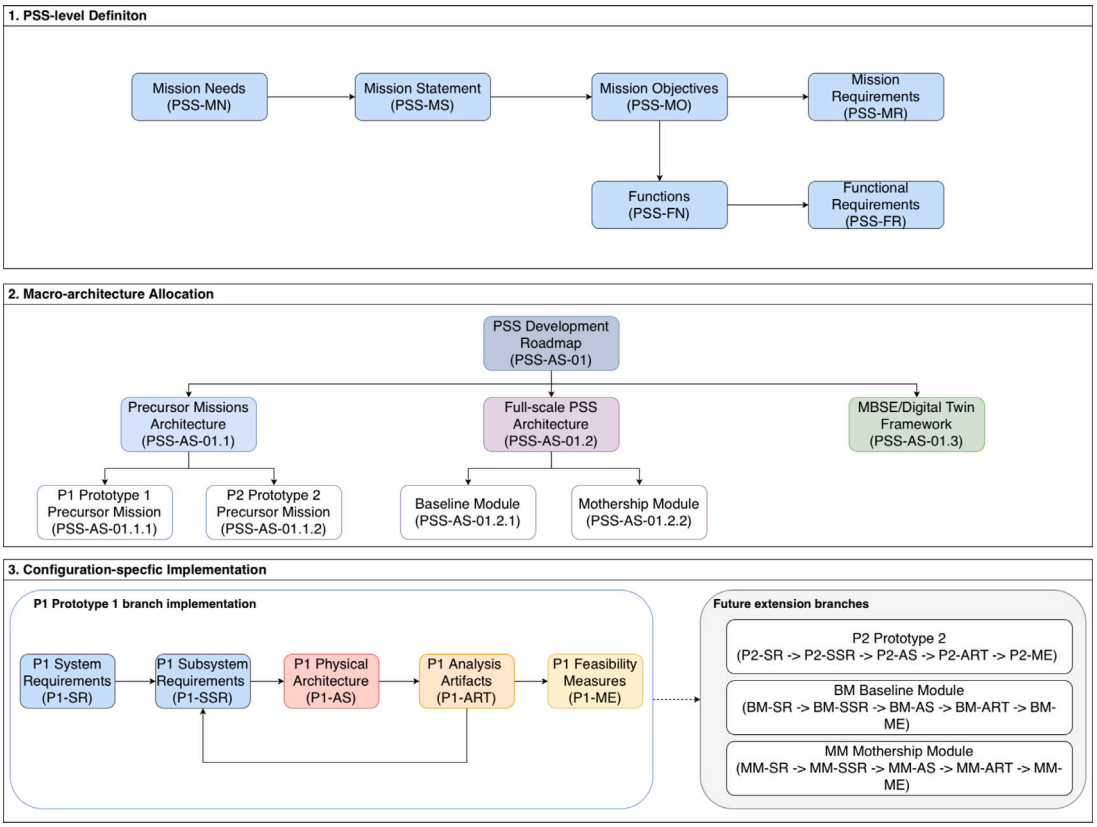

Fig. 1. MBSE requirements flowdown adopted for the modular PSS feasibility assessment.

Table 1
Reference configuration families and communication roles.

Configuration	Role	Communication capability
P1	Precursor demonstrator	Earth link
P2	Larger-scale demonstrator	ISL + Earth link
BM	PSS modular unit	ISL
MM	Coordination/relay element	Earth link + ISL

The configuration families and their communication roles are summarized in Table 1. In this work, P1 is developed in detail as the first configuration-specific application of the MBSE framework that will be introduced in Section 3. P2, the BM, and the MM are retained as reference configuration families and future extensions of the same framework.

3. Model-based systems engineering framework

The modular PSS architecture introduced in Section 2 requires a traceable engineering process able to connect the different levels of the feasibility assessment. This is particularly relevant because the PSS is not a conventional single-spacecraft mission, but a distributed, scalable, and long-term architecture that must be progressively developed through precursor missions and modular configurations.

To support this process, an MBSE framework is developed for the feasibility assessment of the modular PSS concept. In this work, MBSE is adopted to structure the assessment around connected models of requirements, architecture, and analysis. This is consistent with the International Council on Systems Engineering (INCOSE) view of MBSE as a lifecycle-oriented modeling approach supporting requirements definition, design, analysis, and verification activities from the early design phases onward [15].

The adopted flowdown is tailored from established space systems-engineering practices. In the NASA Systems Engineering Handbook [16], requirements flowdown is represented from mission objectives and mission requirements toward system functional and performance requirements, subsystem requirements, and allocated or derived requirements. Consistently with this logic, the present framework starts from PSS mission needs and mission objectives, derives mission requirements, functions, and functional requirements, and then connects them to configuration-specific requirements and verification artifacts. The requirement derivation, allocation, and verification links are defined consistently with European Cooperation for Space Standardization (ECSS) system engineering requirements and traceability principles [17].

MBSE has been widely investigated in space applications and has been applied to small-satellite and CubeSat mission design to support requirements traceability, architecture definition, simulation integration, and preliminary design activities [18–21]. However, its application to modular PSS development remains less mature.

The proposed framework is implemented within an MBSE Digital Twin-oriented environment used to organize the feasibility assessment as an updateable engineering process. Requirements and architecture elements are linked to parametric sizing and analysis artifacts. The resulting outputs are stored as measures, enabling the impact of future changes in assumptions, configurations, or subsystem selections to be traced through the framework. At this stage, the framework should not be interpreted as a fully operational Digital Twin. Nevertheless, it implements several capability-oriented elements that are consistent with the Digital Twin Capabilities Periodic Table [22], which organizes Digital Twin development around use-case capability requirements rather than vendor-specific technologies. Therefore, in this work, the term Digital Twin-oriented refers to a structured digital-engineering environment that links requirements, architecture, sizing models, simulation artifacts, and feasibility measures. These capabilities provide the basis for progressively extending the framework toward a more mature Digital Twin as new assumptions, analysis results, precursor mission data, and operational feedback become available.

Table 2
Representative high-level PSS mission logic used in the MBSE framework.

Level	ID	Representative statement
Mission need	PSS-MN-01	Need for space-based solar shading to reduce a fraction of the incoming solar radiation reaching Earth.
Mission need	PSS-MN-02	Need for a modular and scalable PSS architecture.
Mission objective	PSS-MO-01	Assess the feasibility of a modular PSS architecture through the definition, sizing, and analysis of a representative modular unit.
Mission objective	PSS-MO-03	Define prototype configurations to demonstrate key technologies required for progressive modular PSS development.
Functional requirement	PSS-FR-01	The PSS shall provide controlled solar-shading capability.
Functional requirement	PSS-FR-03	The PSS shall support communication and coordination among architecture elements.

3.1. Framework rationale and scope

The framework was developed to address four main needs: traceability across mission, architecture, requirements, analysis, and measures; separation between PSS-level logic and configuration-specific implementations; integration of sizing and analysis artifacts; and updateability of quantitative feasibility measures. This is particularly important when moving from the full-scale PSS concept to precursor configurations and individual modular elements, since configuration design choices must remain linked to the higher-level modular architecture while avoiding the direct transfer of final-system requirements to early demonstrators.

The framework is organized in three connected levels. The first level defines the high-level PSS mission logic, including mission needs, mission statement, mission objectives, mission requirements, functions, and functional requirements. The second level allocates the PSS-level functional requirements to macro-architecture elements, preserving the distinction between the full-scale PSS architecture and precursor mission configurations. The third level introduces configuration-specific implementation branches, where system and subsystem requirements are linked to physical architecture elements, analysis artifacts, and feasibility measures.

Fig. 1 summarizes the logical flowdown adopted in the MBSE framework. The figure reports the flowdown direction used to organize the model, while the formal relationship types implemented in the MBSE environment include trace, refine, derive, satisfy, verify, source, and specify links.

PSS-level requirements flowdown. At the PSS level, the model starts from the mission needs and mission statement, which define the overall rationale of the modular PSS feasibility framework. The mission objectives refine this rationale and are used to derive mission requirements and guide the functional analysis.

The functional analysis identifies the main functions required to satisfy the mission objectives. These functions are then used to derive the PSS-level functional requirements, which provide the link between the high-level mission logic and the subsequent architecture allocation. This flowdown ensures that the functional requirements used for architecture allocation remain traceable to the original mission rationale.

Macro-architecture allocation. Once the PSS-level functional requirements are defined, they are allocated to the macro-architecture elements. These macro-assets include the Precursor Missions Architecture, the Full-scale PSS Architecture, and the MBSE/Digital Twin Framework. The Precursor Missions Architecture includes P1 and P2 as progressive demonstration configurations. The Full-scale PSS Architecture includes the BM and the MM as target architecture elements. This allocation step connects the PSS-level functional logic to the reference architecture while preventing the direct assignment of general PSS-level requirements to prototype-specific subsystems.

Configuration-specific implementation branch. After macro-architecture allocation, the framework is extended into configuration-specific implementation branches. In principle, this structure can be applied to several configurations, including P1, P2, the BM, and the MM. In the present paper, P1 is selected as the detailed application case, while the other branches are retained as future extensions of the same framework.

Within the P1 branch, system requirements are derived from the PSS-level functional requirements. They are then refined into subsystem requirements through an iterative process involving parametric sizing and analysis artifacts. The P1 subsystem requirements are linked to P1 physical architecture elements and verified through analysis artifacts and budget models. These artifacts include, for example, the mass budget, power budget, communication link budget, AOCS torque analysis, sail sizing, and configuration assessment. Their numerical outputs are stored in the MBSE model as feasibility measures. The resulting traceability chain connects PSS-level functional requirements to P1 system requirements, subsystem requirements, physical architecture elements, analysis artifacts, and measures. This chain allows each feasibility measure obtained for P1 to be traced back to the PSS-level functional logic. It should be noted that the chain is not purely linear: in the preliminary design phase, parametric sizing and analysis artifacts can also refine quantitative subsystem-level requirements. This iterative loop is represented in Fig. 1 by the return arrow from analysis artifacts to P1 subsystem requirements.

Cross-configuration demonstration traceability. To support the progressive development of the PSS architecture, the framework also introduces traceability between precursor demonstration objectives and subsequent configurations. Demonstration objectives are linked to the PSS-level functional logic and to the configuration-specific requirements, analysis artifacts, and feasibility measures that provide supporting evidence. The same objectives can then be traced to subsequent configurations for which the resulting evidence is relevant. This cross-configuration traceability is intended to identify which precursor results can inform later design stages while explicitly preserving the limits of representativeness of each demonstration. In this way, the framework provides a model-based basis for assessing the relevance of precursor demonstrations to the target architecture. The approach is illustrated for P1 in Section 4, while the detailed P2, BM, and MM implementation branches remain subject to future development.

3.2. Parametric sizing and analysis integration

Parametric sizing and analysis artifacts are integrated into the MBSE model to support the feasibility assessment. These artifacts are represented in the model and linked to the requirements they verify, as well as to the relevant architecture elements or subsystems.

The numerical outputs of the analyses are stored as measures. Examples include total mass, power demand, link margin, data rate, solar sail area, stowed volume, and required control torques. In this sense, the analysis artifacts do not only verify requirements, but also support the refinement of quantitative subsystem-level thresholds.

The feasibility results are therefore interpreted as reference measures obtained under a defined set of assumptions, rather than as a fixed final design. Since the sizing models are parametric, assumptions such as sail size, subsystem power demand, communication architecture, actuator selection, margin policy, or configuration constraints can be modified and re-evaluated. The MBSE framework preserves the traceability of these updates to the requirements, architecture elements, analysis artifacts, and measures. This makes the framework suitable for iterative comparison between configurations and for future extension toward P2, the BM, and the MM.

Table 3
P1 demonstration objectives and associated sub-objectives.

ID	Demonstration objective
P1-DO-01	Scalable system operations in the vicinity of L_1^*.
P1-DO-01.1	Demonstrate solar-sail-based orbit maintenance and station keeping near L_1^*.
P1-DO-01.2	Demonstrate and characterize attitude and orientation control near L_1^*.
P1-DO-02	Long-term performance of the optical sail material in the L_1^* environment.
P1-DO-02.1	Characterize the degradation of the optical properties of the sail material under L_1^* environmental exposure.
P1-DO-02.2	Characterize the mechanical resilience and environmental response of the sail material in the L_1^* environment.
P1-DO-02.3	Assess the impact of optical degradation on SRP-driven trajectory and attitude-control performance.

3.3. MBSE implementation and model entities

The framework was implemented in Innoslate as the supporting MBSE platform. Separate model documents were created for mission needs, mission objectives, mission requirements, functions, PSS-level functional requirements, P1 system requirements, and P1 subsystem requirements. This organization preserves the separation between the PSS-level mission logic and the configuration-specific P1 implementation, while allowing requirements, architecture elements, analysis artifacts, and feasibility measures to be connected through traceability relationships.

Table 2 reports a representative set of the high-level mission logic used to illustrate the flowdown adopted in the MBSE framework. The complete set of mission needs, objectives, requirements is implemented in the MBSE model and used to support the traceability relationships described in this section. Section 4 applies the framework to P1 as the first detailed precursor implementation of the modular PSS concept.

4. Prototype 1 as framework application case

P1 is the configuration-specific application case of the MBSE framework described in Section 3. The configuration is based on the precursor mission concept developed in previous work [10]. The precursor mission was defined around two main demonstration objectives: scalable system operations in the vicinity of L_1^*, including solar-sail-based attitude and orbit control, and the assessment of the long-term performance of the optical shield material in the L_1^* environment. Within the MBSE model, these objectives are represented through the P1 demonstration-objective hierarchy summarized in Table 3. In the present work, this concept is reformulated within the proposed MBSE framework to support a traceable feasibility assessment.

P1 is a precursor demonstrator based on CubeSat-class and near-term technologies. Its purpose is to address these demonstration objectives at a reduced scale before moving toward larger precursor configurations or target module architectures. It is therefore not treated as a final PSS module, but as an early demonstrator used to evaluate the feasibility of selected technologies and design assumptions relevant to the modular architecture.

4.1. P1 parametric sizing and analysis model

The preliminary feasibility assessment of P1 is performed through a parametric sizing model implemented as an analysis artifact and connected to the MBSE environment. The purpose of the model is to provide a flexible and updateable sizing capability able to translate reference assumptions into quantitative feasibility measures. In this way, changes in sail size, material properties, subsystem masses, power demand, communication assumptions, or margin policy can be reflected in the corresponding mass, volume, power, communication, and AOCS-related outputs.

The parametric model is initialized from reference mission and configuration inputs derived from the precursor mission study, literature values, preliminary architectural choices, and simplified analytical relationships. The resulting outputs are stored in the MBSE model as measures and linked to the corresponding P1 requirements, physical architecture elements, and analysis artifacts.

4.1.1. Reference mission and trajectory assumptions

The first sizing iteration uses the reference trajectory from the precursor mission study [10] as the initial mission input for P1. This trajectory provides the starting point for the parametric sizing process, while the resulting feasibility measures can be fed back into later iterations to update the trajectory assumptions, configuration definition, and subsystem design.

The reference orbit is modeled within the photo-gravitational Sun-Earth/ Moon CoM Circular Restricted Three-Body Problem (PCR3BP) and is located in the vicinity of the artificial equilibrium point L_1^*, shifted sunward with respect to the classical L_1 point because of solar radiation pressure (SRP). The adopted ideal lightness parameter is $\beta = 0.0349$, which places L_1^* at approximately $d_{E-L_1^*} = 2.364 \times 10^6$ km from Earth.

A barycentric synodic reference frame $\mathcal{F}_s = \{\hat{\mathbf{x}}, \hat{\mathbf{y}}, \hat{\mathbf{z}}\}$ is adopted, with the origin located at the CoM of the Sun–Earth/Moon system. The $\hat{\mathbf{x}}$-axis is aligned with the Sun–Earth/Moon CoM line, the $\hat{\mathbf{z}}$-axis is aligned with the angular momentum vector of the system, and the $\hat{\mathbf{y}}$-axis completes the right-handed frame.

The reference trajectory provides the sail cone and clock angle histories, $\alpha(t)$ and $\delta(t)$, used as attitude inputs for the preliminary AOCS torque assessment. In the adopted reference frame, the cone angle α is defined as the angle between the sail normal unit vector $\hat{\mathbf{n}}$ and the $\hat{\mathbf{x}}$ direction, while the clock angle δ is defined as the angle between the projection of $\hat{\mathbf{n}}$ onto the $\hat{\mathbf{y}} - \hat{\mathbf{z}}$ plane and the $\hat{\mathbf{y}}$ direction. The Earth–spacecraft distance along the reference trajectory is also used in the communication link-budget assessment.

4.1.2. Reference configuration and sizing assumptions

The reference P1 configuration is initialized as a CubeSat-class solar-sail demonstrator with direct Earth communication capability. The main configuration input is a square reflective sail with side length $L_{\text{sail}} = 20$ m, corresponding to a deployed sail area of $A_{\text{sail}} = 400$ m^2. The sail is assumed to be supported by four deployable booms connected to a central bus.

The sail membrane areal density is an input parameter referring to the reflective membrane only. Literature values for modern solar-sail membranes are typically in the range of 1 g/m^2 up to about 20 g/m^2 [23–26]. Based on this range, the P1 sizing model adopts a preliminary sail areal density of $\sigma_{\text{sail}} = 5$ g/m^2. The adopted value is also consistent with order-of-magnitude values reported for previous and recent solar-sail demonstrator concepts, including Cosmos 1 and ACS3 [24,27].

The sail packing efficiency is defined as the ratio between deployed sail area and stowed sail volume, including the sail support structure and deployment mechanism. Recent space-sail reviews report an order-of-magnitude improvement in achievable deployed-area-to-stowed-volume ratios, from approximately 10^3–10^4 m^2/m^3 to values close to 10^5 m^2/m^3 [28]. Based on this trend, a reference packing efficiency of $\eta_{\text{pack}} = 5 \times 10^4$ m^2/m^3 is adopted for the P1 sizing model.

The sail is assumed to be supported by four booms extending from the central bus to the sail corners. For the square reference geometry, the single-boom length is $L_{\text{boom}} = \sqrt{2}L_{\text{sail}}/2 = 14.14$ m. The boom linear density is set to $\lambda_{\text{boom}} = 0.1$ kg/m. This value is consistent with representative solar-sail hardware concepts reported by Herbeck

et al. [24], where specific boom masses of approximately 100–120 g/m are listed for several square-sail designs. Although lower values have been reported for lightweight boom concepts, the value adopted here is retained as a conservative preliminary sizing assumption to avoid underestimating boom mass, inertia, and AOCS torque requirements.

An initial bus allocation of $m_{\text{bus}} = 9$ kg is adopted to initialize the reference mass, consistently with the precursor reference configuration. For the preliminary inertia estimate, the bus is approximated as a rectangular prism with dimensions representative of a 12U CubeSat-class spacecraft, with $L_{1,\text{bus}} = 0.366$ m and $L_{2,\text{bus}} = L_{3,\text{bus}} = 0.2263$ m.

For the preliminary SRP and disturbance-torque assessment, an overall sail thrust coefficient $\eta = 1.8$ is adopted to represent a highly reflective but non-ideal solar-sail surface, while the ideal perfectly reflecting limit is $\eta = 2$. A CoM–CoP offset equal to 0.25% of the sail side length is assumed as a nominal worst-case condition, following assumptions used in previous studies [29,30]. For the 20 m × 20 m P1 sail, this corresponds to $r_{\text{off}} = 0.05$ m.

4.1.3. First-iteration sizing outputs

Based on the reference inputs and assumptions defined above, the first sizing iteration provides the main sail, boom, packaging, mass, area-to-mass, and inertia-related quantities used to initialize the P1 feasibility assessment. These outputs are not intended to define a final spacecraft configuration, but to provide a consistent reference case for the subsequent AOCS, design budget, communication, and MBSE traceability analyses.

The reflective sail membrane mass is computed as

$$m_{\text{sail}} = \sigma_{\text{sail}} A_{\text{sail}} = 2.0 \text{ kg}. \tag{1}$$

The stowed sail volume is estimated from the adopted packing efficiency as

$$V_{\text{stowed}} = \frac{A_{\text{sail}}}{\eta_{\text{pack}}} = 8.0 \times 10^{-3} \text{ m}^3. \tag{2}$$

For the four-boom configuration, the total boom mass is computed as

$$m_{\text{booms}} = 4 \lambda_{\text{boom}} L_{\text{boom}} = 5.65 \text{ kg}. \tag{3}$$

Combining the reflective sail membrane, boom system, and reference bus allocation gives the first reference mass:

$$M_{\text{ref}} = m_{\text{sail}} + m_{\text{booms}} + m_{\text{bus}} = 16.65 \text{ kg}. \tag{4}$$

For the deployed sail area of 400 m^2, this corresponds to an initial area-to-mass ratio:

$$\left(\frac{A}{M}\right)_{\text{ref}} = \frac{A_{\text{sail}}}{M_{\text{ref}}} = 24.0 \text{ m}^2/\text{kg}. \tag{5}$$

For the preliminary AOCS sizing, the inertia tensor of the P1 configuration is estimated using a simplified rigid-body model. A body-fixed reference frame $\mathcal{F}_b = \{\hat{\mathbf{x}}_b, \hat{\mathbf{y}}_b, \hat{\mathbf{z}}_b\}$ is defined with the $\hat{\mathbf{x}}_b$-axis aligned with the sail normal direction and the $\hat{\mathbf{y}}_b, \hat{\mathbf{z}}_b$ axes lying in the sail plane. Under the adopted symmetric mass-distribution assumption, $\mathcal{F}_b$ is also used as the principal-inertia frame.

The spacecraft is represented as the combination of a thin square sail membrane, four supporting booms modeled as beam elements, and a central bus modeled as a rectangular prism. The preliminary mass model assumes a symmetric reference configuration, with the sail, booms, and bus aligned with the body-fixed frame. The total CoM is computed from the sail, boom, and bus mass contributions, and the component inertias are referred to this CoM using the parallel-axis theorem.

For the reference P1 configuration, the resulting inertia tensor is

$$\mathbf{I} = \begin{bmatrix} 510.53 & 0 & 0 \\ 0 & 255.51 & 0 \\ 0 & 0 & 255.51 \end{bmatrix} \text{kg m}^2.$$

Table 4 summarizes the main outputs for the P1 configuration, used in the subsequent subsystem sizing.

Table 4
Main outputs of the first P1 sizing iteration.

Quantity	Value	Note
Deployed sail area	400 m^2	20 m × 20 m sail
Sail membrane mass	2.0 kg	Reflective membrane only
Stowed sail volume	8.0×10^{-3} m^3	From packing efficiency
Single-boom length	14.14 m	Center-to-corner boom
Total boom mass	5.65 kg	Four-boom configuration
Reference bus allocation	9.0 kg	Initial bus/deployment value
Reference mass	16.65 kg	Sail + booms + bus allocation
Initial area-to-mass ratio	24.0 m^2/kg	Reference sizing value
I_{xx}	510.53 kg m^2	Sail-normal axis
$I_{yy} = I_{zz}$	255.51 kg m^2	In-plane axes

4.1.4. Preliminary AOCS torque assessment

The AOCS sizing model uses the geometric, mass, inertia, and sail parameters obtained from the first sizing iteration to derive preliminary attitude-control requirements for P1. The objective is to estimate the order of magnitude of the required control authority and to compare it with representative actuator families.

The preliminary attitude-reconstruction and torque-evaluation approach follows the methodology developed in [31]. The attitude history is obtained from the cone and clock angles associated with the reference trajectory. The corresponding ideal attitude-tracking torque is computed from Euler's equation,

$$\boldsymbol{\tau}^b_{\text{ideal}} = \mathbf{I}^b \dot{\boldsymbol{\omega}}^b + \boldsymbol{\omega}^b \times \left(\mathbf{I}^b \boldsymbol{\omega}^b\right), \tag{6}$$

where $\mathbf{I}^b$ is the preliminary inertia tensor of the P1 configuration and $\boldsymbol{\omega}^b$ is the angular velocity history expressed in the body frame. $\boldsymbol{\tau}^b_{\text{ideal}}$ represents the torque required to follow the prescribed attitude history in the absence of external disturbances.

A separate disturbance-rejection case is evaluated by considering the SRP force acting on the sail and the assumed CoM–CoP offset. The SRP force magnitude is approximated using a simplified non-perfect solar-sail model,

$$F_{\text{SRP}} = \eta P A_{\text{sail}} \cos^2 \alpha, \tag{7}$$

where P is the solar radiation pressure at the sail heliocentric distance, defined as

$$P = \frac{P_0}{r^2}, \qquad P_0 = 4.56 \times 10^{-6} \text{ N m}^{-2}. \tag{8}$$

Here, P_0 is the SRP at 1 AU, r is the Sun–sail distance normalized by 1 AU, and η is the overall sail thrust coefficient. A value $\eta = 1.8$ is adopted to account for non-ideal sail-surface behavior, while the ideal perfectly reflecting limit is $\eta = 2$. In the preliminary worst-case estimate, the maximum SRP force is evaluated and assumed to act along the sail-normal direction.

The disturbance torque due to the assumed CoM–CoP offset is computed as

$$\boldsymbol{\tau}^b_{\text{SRP}} = \mathbf{r}^b_{\text{off}} \times \mathbf{F}^b_{\text{SRP}}. \tag{9}$$

For the 20 m × 20 m P1 sail, the reference offset is

$$r_{\text{off}} = 0.0025 \times L_{\text{sail}} = 0.05 \text{ m}. \tag{10}$$

The offset is assumed to lie in the sail plane. To obtain a conservative component-wise estimate of the in-plane disturbance-rejection requirement, an offset component of 0.05 m is considered along the in-plane axes.

For the reference configuration, the maximum SRP force is

$$F_{\text{SRP}} = 3.39 \times 10^{-3} \text{ N}, \tag{11}$$

leading to an SRP disturbance torque of

$$\tau_{\text{SRP}} = 1.69 \times 10^{-4} \text{ Nm}. \tag{12}$$

Table 5
Preliminary AOCS torque requirements for the P1 reference configuration.

Quantity	Value
Maximum ideal attitude-tracking torque	2.11×10^{-10} Nm
SRP disturbance torque	1.69×10^{-4} Nm
Required in-plane torque	3.39×10^{-4} Nm
Required about-normal torque	8.47×10^{-6} Nm

A design margin factor $M_\tau = 2$ is applied to obtain the preliminary in-plane disturbance-rejection requirement:

$$\tau_{\mathrm{ip,req}} = M_\tau \tau_{\mathrm{SRP}} = 3.39 \times 10^{-4}\ \mathrm{Nm}. \tag{13}$$

Following the preliminary worst-case estimate reported in [32], the about-normal torque requirement is assumed to be 1/40 of the in-plane disturbance-rejection requirement:

$$\tau_{\mathrm{n,req}} = \frac{1}{40}\tau_{\mathrm{ip,req}} = 8.47 \times 10^{-6}\ \mathrm{Nm}. \tag{14}$$

This term can be considered as a conservative value for non-ideal SRP effects, actuator asymmetries, deployment imperfections, and future control configurations. For the reference P1 trajectory, the maximum ideal attitude-tracking torque is approximately 2.11×10^{-10} Nm, which is several orders of magnitude smaller than the SRP-induced disturbance torque. Therefore, the preliminary AOCS sizing is driven by the disturbance-rejection case rather than by the ideal attitude-tracking torque.

Table 5 summarizes the preliminary AOCS torque requirements for the P1 reference configuration.

4.2. Subsystem selection and preliminary design budgets

4.2.1. AOCS actuator feasibility assessment

The resulting requirements are then used to perform a preliminary actuator feasibility check to assess whether representative actuator families can provide torque authority of the same order as the preliminary disturbance-rejection requirements.

Reaction wheels are included as the baseline high-accuracy attitude-control option. They provide three-axis control authority and high pointing precision, but require momentum management. A representative CubeSat-class unit, the AAC Clyde Space RW400, is used for the preliminary feasibility comparison. The selected RW400 configuration provides a maximum torque of 8 mNm, an angular momentum storage of 15 mNms, a maximum speed of 5000 rpm, and a mass of 0.197 kg [33]. These values are compared against the preliminary torque requirements derived for P1.

Tip-mounted control vanes are included as candidate actuator concepts for SRP-based attitude control. They consist of reflective surfaces located near the sail tips, whose deflection modifies the local SRP force direction and generates control torques about the spacecraft CoM. In the present P1 model, the tip-vane geometry is used as a simplified preliminary sizing assumption to estimate the available SRP-induced torque authority. A triangular vane geometry with base and height equal to 2 m is assumed. The vane tilt and twist deflection angles are both set to 45°. Under this assumption, the four-vane configuration provides an estimated in-plane torque of 1.77×10^{-4} Nm in the tilt-only case and 3.55×10^{-4} Nm when both tilt and twist contributions are considered. The latter value is comparable to the required in-plane disturbance-rejection torque of 3.39×10^{-4} Nm. Therefore, tip vanes are retained as a potentially feasible SRP-based actuator family for in-plane disturbance rejection, while requiring further structural, deployment, and controllability analysis in future design iterations.

Active Mass Translation (AMT) is considered as a candidate in-plane momentum management concept. AMT generates control authority by shifting the spacecraft CoM relative to the CoP. AMT has been implemented in the NEA Scout solar-sail mission as part of the attitude control and momentum management architecture [34]. Solar Cruiser studies also consider AMT as one of the primary momentum management actuators, with a system translating approximately 50% of the spacecraft mass within a travel range of ±0.29 m [32]. In the present preliminary model, a maximum AMT displacement of $\Delta r_{\mathrm{AMT}} = 0.5$ m is assumed as a first-order sizing value.

The sail assembly is assumed to include both the reflective membrane and the booms. Therefore, the effective CoM displacement is approximated as

$$\Delta r_{\mathrm{CM}} = \Delta r_{\mathrm{AMT}} \frac{m_{\mathrm{sail}} + m_{\mathrm{booms}}}{m_{\mathrm{sail}} + m_{\mathrm{booms}} + m_{\mathrm{bus}}}. \tag{15}$$

The corresponding AMT torque authority is estimated as

$$\tau_{\mathrm{AMT}} \simeq F_{\mathrm{SRP}} \Delta r_{\mathrm{CM}}. \tag{16}$$

Using $\Delta r_{\mathrm{AMT}} = 0.5$ m and the reference sizing values, the estimated AMT torque authority is

$$\tau_{\mathrm{AMT}} = 7.78 \times 10^{-4}\ \mathrm{Nm}. \tag{17}$$

This value is larger than the required in-plane disturbance-rejection torque. AMT is therefore retained as a promising in-plane actuator concept, although further work is required to assess the mechanism mass, moving-mass dynamics, structural integration, and control performance.

Reflectivity Control Devices (RCDs) are considered as a distributed SRP-based actuation concept for solar-sail attitude control. RCDs locally modify the optical properties of selected sail regions, thereby changing the SRP force distribution and generating control torques through the resulting CoM variation. This concept has flight heritage from IKAROS [35], which demonstrated attitude control capability using liquid-crystal reflectivity control devices, and has also been investigated in solar-sail attitude control studies [36]. In the present P1 model, a simplified distributed RCD layout is used as an exploratory sizing case. The sail perimeter is discretized into $N_{\mathrm{RCD}} = 16$ elements, with four elements placed along each side of the sail. Each RCD element is assigned a representative active area, position vector, local tilt angle, and ON/OFF reflectivity state. The adopted layout distinguishes between edge and middle RCD elements as in [36], with local tilt angles $\theta_{\mathrm{edge}} = 15°$ and $\theta_{\mathrm{middle}} = -10°$, respectively.

The torque generated by the active RCD elements is estimated as

$$\boldsymbol{\tau}^b_{\mathrm{RCD}} = \sum_{i=1}^{N_{\mathrm{RCD}}} \mathbf{r}^b_i \times \mathbf{F}^b_{\mathrm{RCD},i}. \tag{18}$$

The RCD torque authority is evaluated over a limited set of representative ON/OFF activation patterns. The values reported here are component-wise maximum torque authorities obtained among the explored configurations. For the explored ON/OFF configurations, the maximum absolute torque components obtained from the RCD sizing model are 2.63×10^{-4} Nm about the sail-normal axis, 9.71×10^{-4} Nm about one in-plane axis, and 2.47×10^{-3} Nm about the other in-plane axis. These values are larger than the preliminary about-normal requirement and comparable or larger than the required in-plane disturbance-rejection torque. RCDs are therefore retained as a promising SRP-based actuator family for future P1 AOCS iterations. However, the present sizing remains exploratory and does not include detailed optical modeling, switching dynamics, structural flexibility, thermal constraints, or electrical power demand.

Table 6 summarizes the preliminary AOCS actuator feasibility assessment for the P1 reference configuration.

The feasibility assessment indicates that the preliminary torque requirements are not prohibitive for the P1 reference configuration. Reaction wheels provide the most mature high-accuracy option, but require momentum management or desaturation under persistent SRP disturbance torques. Their sizing can also become increasingly demanding for larger sail areas, due to the growth of SRP-induced disturbance

Table 6
Preliminary AOCS actuator feasibility assessment for P1.

Actuator concept	Estimated torque authority
Reaction wheels	8.0×10^{-3} Nm
Tip vanes	3.55×10^{-4} Nm
AMT	7.78×10^{-4} Nm
RCDs	Up to 2.47×10^{-3} Nm

torques, angular-momentum accumulation, and spacecraft inertia. SRP-based concepts, including tip vanes, AMT, and RCDs, provide torque authority of the same order or larger than the derived disturbance-rejection requirements. Therefore, the present assessment identifies reaction wheels, tip vanes, AMT, and RCDs as candidate actuator families for future higher-fidelity AOCS design iterations.

4.2.2. Preliminary mass, power, and communication budgets

Following the reference sizing and preliminary AOCS torque assessment, a first-order subsystem sizing is performed to estimate the main spacecraft design budgets for P1. The objective is to verify the compatibility of the reference architecture with representative CubeSat-class subsystems and to close preliminary mass, power, communication budgets.

P1 configuration includes a 12U-class spacecraft bus, a reflective sail membrane supported by four deployable booms, a CubeSat-class C&DH unit, an EPS composed of deployable solar panels and a battery pack, a preliminary S-band communication link, and an AOCS architecture including reaction wheels, attitude sensors, and candidate SRP-based momentum-management devices. These assumptions define the subsystem baseline used for the preliminary mass, power, communication, and AOCS feasibility budgets.

The component-level values used in the subsystem budget are grouped into Commercial Off-The-Shelf (COTS)-based values, literature-based estimates, and preliminary design allocations. The component-level mass and power allocations used to obtain the preliminary budgets are summarized in Appendix A. COTS-based values are taken from publicly available CubeSat product information and datasheets, with EnduroSat [37] components used as representative references for several avionics, EPS, structure, and communication entries. Values not tied to a final selected hardware unit at this stage, such as AMT, RCDs, attitude sensors, and monitoring sensors, are treated as first-order allocations. The sail membrane and boom properties are instead derived from the sizing model described before. The AMT and RCD entries are included in the spacecraft-level budget as preliminary mass and power allocations.

The communication subsystem is preliminarily sized using an S-band baseline link to Earth. The selected reference transceiver supports an RF output power up to 33 dBm, corresponding to approximately 2 W, and a configurable data-rate range up to 125 kbps. The communication need is estimated from the types of data expected to be generated and transmitted by the precursor mission. Based on the preliminary data budget developed in previous work [10], housekeeping and telemetry require low data rates of a few kbps, whereas payload data were preliminarily estimated in the range of 50–200 kbps during data-intensive operations. For the present preliminary feasibility assessment, the 20 kbps case is therefore retained as a reference low-rate link for housekeeping, telemetry, diagnostics, and selected monitoring data. Higher-rate monitoring or payload-data return is retained as a future communication-architecture driver.

A preliminary link budget is computed using the standard formulation reported in Space Mission Analysis and Design [38]. The analysis assumes an S-band downlink to Earth, a 5 dBi spacecraft antenna gain, a DSN 34-m BWG S-band receiving gain of approximately 57 dBi, and a maximum Earth–spacecraft distance of 2.36×10^6 km. Under the adopted antenna, loss, and receiver assumptions, a 20 kbps reference data-rate case closes with a preliminary positive link margin of approximately 1.55 dB. The reference S-band link-budget parameters are reported in Appendix B. The S-band link is therefore retained as a first-order feasibility assessment for low-rate TT&C, telemetry, and diagnostic data return. Higher-data-rate communication may be addressed in future iterations through an additional X-band downlink transmitter, while retaining the S-band transceiver for TT&C and basic telemetry. A preliminary X-band sensitivity case, assuming a 2 W RF output power, a 12 dBi spacecraft antenna gain, and a DSN 34-m X-band receiving gain of approximately 68 dBi, indicates that a 50 kbps downlink could close with positive margin under the adopted assumptions. This option requires a dedicated future trade-off.

Table 7
Preliminary design budgets for the P1 reference configuration.

Budget item	Value
Avionics mass	16.79 kg
Total mass, including sail subsystem	24.44 kg
Margin	20%
Total mass with margin	29.33 kg
Nominal power	23.71 W
Peak power	54.80 W
Peak power with margin	65.76 W
Generated power	76.80 W

The preliminary component allocations lead to the design budgets summarized in Table 7.

It should be noted that the mass used in the first sizing iteration and the mass obtained from the subsystem budget are not identical quantities. The reference mass, $M_{\mathrm{ref}} = 16.65$ kg, includes only the sail membrane, four booms, and a preliminary bus allocation. This value is used to initialize the area-to-mass ratio, inertia estimate, and AOCS disturbance assessment. The subsystem budget then refines the spacecraft mass by introducing representative subsystem contributions, including avionics, EPS, communications, AOCS hardware, monitoring payload, and sail subsystem elements. This leads to a total mass of 24.44 kg before margin and 29.33 kg after applying the 20% margin. The increase with respect to the simplified precursor reference configuration is mainly due to the inclusion of more complete subsystem-level allocations, including AOCS hardware, communication and EPS components, monitoring payload, structure and deployment-mechanism allowance, and system-level margin. Therefore, the resulting mass should be interpreted as a conservative preliminary budget for the first feasibility-assessment iteration. Future iterations may reduce the total mass through subsystem selection, deployment-mechanism refinement, and optimization of the AOCS architecture.

This distinction reflects the iterative nature of the proposed framework. The first sizing iteration is initialized using the precursor reference trajectory [10]. The updated mass budget is then used to demonstrate a second trajectory iteration. Using the total mass including system-level margin, the area-to-mass ratio becomes

$$\left(\frac{A}{M}\right)_{\mathrm{updated}} = \frac{400}{29.33} = 13.64 \ \mathrm{m^2/kg},$$

leading to an updated lightness parameter of approximately $\beta = 0.0167$. The corresponding nominal photo-gravitational equilibrium point is located at approximately $d_{E-L_1^*} = 1.85 \times 10^6$ km from Earth. These values are then propagated back into the trajectory model to update the associated operating point and generate an updated reference trajectory for the revised P1 configuration.

This second iteration is not intended to represent a finalized trajectory optimization, but to demonstrate how updated feasibility measures can be propagated through the framework. In later design phases, the trajectory, AOCS, communication architecture, and subsystem budgets should be iterated jointly until convergence of the main feasibility measures is achieved.

The updated x–y trajectory and the corresponding cone-angle history are shown in Fig. 2. As in [10] orbit design, the clock-angle

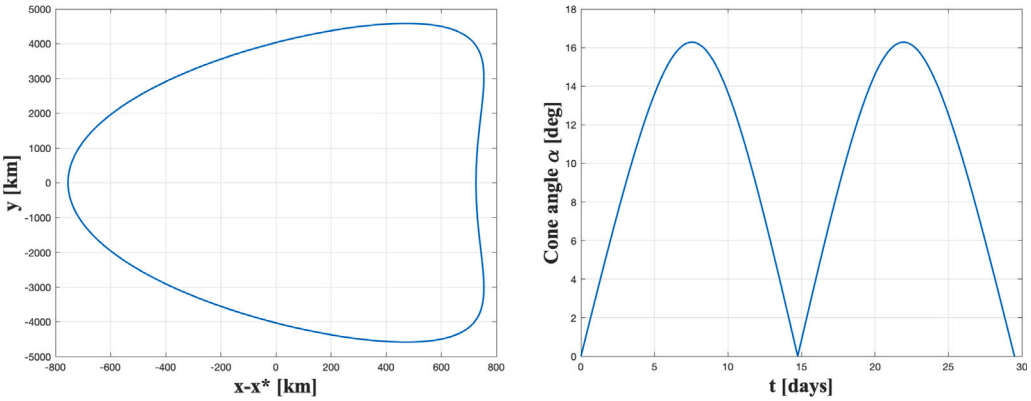

(a) x-y trajectory. (b) Cone angle $\alpha(t)$.

Fig. 2. Updated P1 reference trajectory and cone-angle history obtained from the second trajectory iteration using the mass-updated lightness parameter. The x-y projection is expressed in the co-rotating synodic frame and centered with respect to the associated operating point x^*.

Table 8
Representative derived P1 requirements and associated verification artifacts.

ID	Derived requirement	Artifact
P1-SSR-SAIL-01	The sail subsystem shall provide a deployed reflective area of $A_{\text{sail}} = 400$ m^2.	Sail sizing model
P1-SSR-MASS-01	The reference configuration shall have a total mass not exceeding $M_{\text{tot}} = 29.33$ kg.	Mass budget
P1-SSR-EPS-01	The EPS shall support a peak power demand of 65.76 W.	Power budget
P1-SSR-COM-01	The communication subsystem shall support an Earth-link data rate of at least $R_b = 20$ kbps.	Link budget
P1-SSR-AOCS-01	The AOCS shall provide an in-plane disturbance-rejection torque authority of at least $\tau_{\text{ip,req}} = 3.39 \times 10^{-4}$ Nm.	AOCS torque analysis
P1-SSR-AOCS-02	The AOCS shall provide about-normal control authority of at least $\tau_{\text{n,req}} = 8.47 \times 10^{-6}$ Nm.	AOCS torque analysis

history is not reported as a separate plot, since the clock angle switches between $\delta = 0$ and $\delta = \pi$.

The second trajectory iteration modifies the cone-angle history, but the updated AOCS calculation confirms that the ideal attitude-tracking torque remains of the same order of magnitude so still several orders of magnitude smaller than the SRP-induced disturbance torque. Therefore, the preliminary AOCS sizing remains driven by the conservative SRP disturbance-rejection case.

The updated trajectory also modifies the Earth–spacecraft distance relevant to the communication analysis. Using the maximum Earth–spacecraft distance associated with the updated trajectory, the 20 kbps S-band reference link closes with a positive preliminary margin of approximately 3.68 dB. This confirms that the communication feasibility assessment remains positive when the mass-updated trajectory is considered.

The resulting budgets indicate that the P1 reference configuration remains compatible with a CubeSat-class design philosophy, within the adopted assumptions. The mass budget is mainly driven by the bus-related allocation, AOCS hardware, EPS, sail-supporting booms, and deployment hardware, while the power budget is driven by communication, AOCS, and monitoring-payload operations during peak conditions.

4.3. P1 architecture, derived requirements, and MBSE traceability

Within the MBSE model, P1 system requirements are derived from the PSS-level functional requirements and refined into subsystem-level requirements. These requirements cover the main capabilities needed by the precursor demonstrator, including reflective sail capability, AOCS capability, communication capability, power generation and storage, data handling, monitoring, budget compatibility, and feasibility-data generation. A subset of these derived P1 requirements is reported in Table 8.

The P1 physical architecture is derived from the subsystem requirements and from the preliminary sizing results. It includes the main spacecraft subsystems required for a representative precursor configuration: AOCS, EPS, communication subsystem, structure, C&DH, sail subsystem, and monitoring payload.

The physical architecture provides the system layer used to connect the derived requirements to the corresponding sizing and verification artifacts. In particular, the sail subsystem is linked to the sail and boom sizing model, the AOCS is linked to the torque analysis and actuator feasibility assessment, the communication subsystem is linked to the link-budget analysis, and the EPS and avionics are linked to the power and mass budgets. The resulting P1 physical architecture is shown in Fig. 3.

A representative set of traceability links extracted from the Innoslate model is reported in Table 9. The table summarizes the three relationship types used for the P1 subsystem requirements in the model: *derived by*, *satisfied by*, and *verified by*. These links connect the quantitative subsystem requirements to higher-level capabilities, physical architecture elements, and the sizing or analysis artifacts used for verification.

The feasibility outputs obtained from the sizing and analysis artifacts are stored in the MBSE model as quantitative measures and linked to the corresponding requirements, architecture elements, and verification artifacts. This structure allows changes in design assumptions, such as sail size, membrane areal density, boom linear density, subsystem power demand, actuator selection, communication architecture, or margin policy, to be propagated through the model and traced to the affected system elements.

Therefore, the value of the framework lies not only in the specific numerical results obtained for P1, but also in its ability to support updateable feasibility assessment and future extensions toward P2, the BM, and the MM.

The cross-configuration demonstration traceability introduced in Section 3 is applied here to P1. The two main P1 demonstration objectives refine PSS-MO-03 and are decomposed into the sub-objectives reported in Table 3. These sub-objectives are traced to the P1 system requirements that support their assessment and to the subsequent configurations for which the resulting evidence is relevant. The cross-configuration traces indicate that P1-generated evidence is relevant to subsequent P2 and BM development. The traceability also highlights

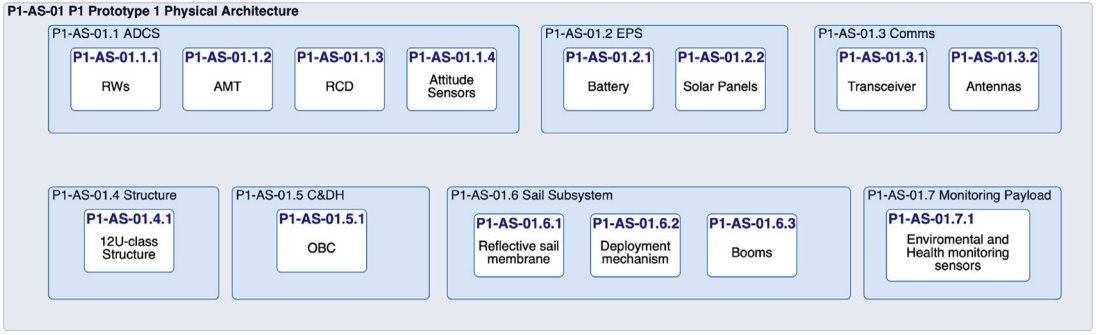

Fig. 3. P1 physical architecture used for MBSE traceability.

Table 9
Representative P1 traceability links extracted from the Innoslate model.

ID	Derived by	Satisfied by	Verified by
P1-SSR-SAIL-01	P1-SR-3 Reflective-sail capability	P1-AS-01.6.1 Sail subsys	P1-ART-02 P1 sizing model
P1-SSR-MASS-01	P1-SR-13 Design budget compatibility	P1-AS-01 P1 physical architecture	P1-ART-02 P1 mass budget
P1-SSR-EPS-01	P1-SR-9 Power generation and storage capability	P1-AS-01.2 EPS	P1-ART-01 P1 power budget
P1-SSR-COM-01	P1-SR-7 Earth communication capability	P1-AS-01.3 Comm subsys	P1-ART-03 P1 link budget
P1-SSR-AOCS-01	P1-SR-5 Attitude-control capability	P1-AS-01.1 AOCS	P1-ART-04 P1 AOCS torque analysis
P1-SSR-AOCS-02	P1-SR-5 Attitude-control capability	P1-AS-01.1 AOCS	P1-ART-04 P1 AOCS torque analysis

Table 10
Representative P1 demonstration-objective traceability links extracted from the Innoslate model.

ID	Higher-level relationship	Traced to P1 system requirements	Cross-configuration trace
P1-DO-01	Refines PSS-MO-03	–	–
P1-DO-01.1	Decomposes P1-DO-01	P1-SR-6 Operational-region support; P1-SR-14 Feasibility-data generation	P2; BM
P1-DO-01.2	Decomposes P1-DO-01	P1-SR-5 Attitude determination and control capability; P1-SR-14 Feasibility-data generation	P2; BM
P1-DO-02	Refines PSS-MO-03	–	–
P1-DO-02.1	Decomposes P1-DO-02	P1-SR-11 Health monitoring capability; P1-SR-14 Feasibility-data generation	P2; BM
P1-DO-02.2	Decomposes P1-DO-02	P1-SR-11 Health monitoring capability; P1-SR-14 Feasibility-data generation	P2; BM
P1-DO-02.3	Decomposes P1-DO-02	P1-SR-5 Attitude determination and control capability; P1-SR-11 Health monitoring capability; P1-SR-14 Feasibility-data generation	P2; BM

full-scale functions that are not represented by P1. No direct cross-configuration trace to the MM is assigned for the demonstration objectives considered here, since distributed multi-spacecraft coordination, inter-satellite communication, data aggregation, and the higher-level coordination and relay functions associated with the MM are outside the P1 demonstration scope. These functions are therefore deferred to subsequent demonstration and implementation branches, including P2, BM, and MM as applicable (see Table 10).

5. Conclusions

This work presented an MBSE framework for the traceable feasibility assessment of a modular Planetary Sunshade System. The framework was developed to support the transition from high-level PSS mission needs and objectives to configuration-specific requirements, architecture elements, parametric sizing artifacts, and quantitative feasibility measures. In this way, the proposed approach provides a structured engineering process for assessing modular PSS configurations while preserving traceability between mission-level rationale, system architecture, subsystem assumptions, and analysis outputs.

The framework was applied to Prototype 1, a representative precursor demonstrator configuration derived from a previous precursor mission concept. The application case showed how reference mission inputs, preliminary spacecraft sizing, AOCS torque assessment, actuator feasibility analysis, design budgets, and derived requirements can be connected within a single updateable feasibility-assessment structure. The resulting P1 configuration includes a 400 m^2 reflective sail area, a total mass below 30 kg, a generated power of 76.80 W, a peak power demand below 55 W, with an Earth-link data-rate reference case of 20 kbps. The preliminary AOCS assessment indicated that the dominant control-sizing driver is associated with SRP disturbance rejection.

The analysis indicates that a Prototype 1 precursor configuration based on CubeSat-class and near-term technologies may be feasible consistently within the adopted assumptions. The updated subsystem mass budget was also propagated back into the trajectory model to demonstrate a second trajectory iteration, showing how revised feasibility measures can be fed back into the framework. At the same time, the results should be interpreted as a preliminary feasibility assessment. Consistently with the parametric nature of the sizing framework, the adopted modeling assumptions are intended to be refined in future iterations. Overall, the proposed framework provides a traceable structure for connecting assumptions, requirements, architecture elements, analysis artifacts, and feasibility measures. This enables design updates to be propagated through the model and provides a basis for comparing different configurations and future extensions. The cross-configuration traceability further makes explicit how the P1 demonstration objectives refine the higher-level PSS mission logic and how the resulting evidence can inform subsequent P2 and BM development.

Future work will focus on improving the fidelity of the parametric models, extending the requirements and verification baseline, integrating additional analyses, and progressively incorporating simulation results and precursor mission data toward a more mature Digital Twin representation of the modular PSS architecture.

Table A.11
Component-level mass and power allocations used for the P1 preliminary budget.

Subsystem	Component or allocation	Mass [kg]	Nominal power [W]	Peak power [W]	Basis
Communication	S-band transceiver	0.246	1.20	12.00	COTS
Communication	S-band patch antennas	0.230	–	–	COTS
C&DH	On-board computer	0.173	0.41	5.00	COTS
EPS	Battery pack and distribution unit	1.478	2.00	2.00	COTS
EPS	Deployable solar panels	1.568	–	–	COTS
Structure and mechanisms	12U-class structure and deployment mechanism	9.000	–	–	Allocation
AOCS	Reaction wheels	0.591	3.00	5.70	COTS
AOCS	Active Mass Translation allocation	0.500	0.50	12.00	Allocation
AOCS	Reflectivity Control Device allocation	0.500	1.00	2.00	Allocation
AOCS	Attitude sensors	2.000	14.60	14.60	Allocation
Sail subsystem	Reflective sail membrane	2.000	–	–	Sizing model
Sail subsystem	Four deployable booms	5.657	–	–	Sizing model
Monitoring payload	Environmental and health-monitoring sensors	0.500	1.00	1.50	Allocation
Total, before margin	–	24.44	23.71	54.80	
System-level margin	–	20%	20%	20%	
Total, with margin	–	29.33	28.45	65.76	

CRediT authorship contribution statement

Marina Coco: Writing – original draft, Visualization, Validation, Methodology, Formal analysis, Conceptualization. **Bruce Chesley:** Supervision. **Marcello Romano:** Supervision. **Chantal Cappelletti:** Supervision.

Declaration of competing interest

The authors declare that they have no known competing financial interests or personal relationships that could have appeared to influence the work reported in this paper.

Acknowledgments

For the author Marina Coco this publication is part of the project PNRR-NGEU which has received funding from the MUR – DM 118/2023. The authors gratefully acknowledge Teaching Science and Technology, Inc. for providing access to the Innoslate license used for the development of the MBSE framework presented in this work. The authors also thank Dr. Giuseppe Governale for valuable discussions.

Appendix A. Supporting sizing and budget assumptions

See Table A.11.

Appendix B. Reference earth-link budget parameters

See Table B.12.

Table B.12
Reference S-band Earth-link budget parameters for the P1 feasibility assessment.

Parameter	Value
Frequency, f	2.2 GHz
RF transmitter power, P_t	2 W
Transmitter line loss, L_l	−1 dB
Spacecraft antenna gain, G_t	5 dBi
Spacecraft antenna HPBW	70°
Transmitter pointing loss, L_{pt}	-2.45×10^{-5} dB
Maximum Earth–spacecraft distance, S	2.36×10^{6} km
Space loss, L_s	−226.76 dB
Propagation and polarization loss, L_a	−0.48 dB
DSN 34-m BWG receiving antenna gain, G_r	56.9 dBi
System noise temperature, T_s	39 K
Reference data rate, R_b	20 kbps
Required E_b/N_0	2.7 dB
Implementation loss	−2.0 dB
Resulting link margin	1.55 dB

References

[1] C. McInnes, Space-based geoengineering: Challenges and requirements, J. Mech. Eng. Sci. 224 (2010) 571–580, http://dx.doi.org/10.1243/09544062JMES1439.
[2] A. Roger, Feasibility of cooling the Earth with a cloud of small spacecraft near the inner Lagrange point (L1), Proc. Natl. Acad. Sci. (PNAS) 103 (46) (2006) 17184–17189, http://dx.doi.org/10.1073/pnas.0608163103.
[3] J. Sánchez, C. McInnes, Optimal sunshade configurations for space-based geoengineering near the sun-earth L1 point, PLoS One 10 (2015) http://dx.doi.org/10.1371/journal.pone.0136648.
[4] F. Oggionni, J. Heiligers, J. Sánchez Cuartielles, Trajectory optimization of a planetary sunshade around the sun-earth L_1 point for solar geoengineering, in: ASCEND 2022, 2022, http://dx.doi.org/10.2514/6.2022-4388.
[5] C.L. Matonti, M. Romano, New families of periodic orbits for solar-sail satellites about photo-gravitational equilibrium points in the restricted two body problem and circular restricted three body problem, Acta Astronautica (2026) http://dx.doi.org/10.1016/j.actaastro.2026.10.012.
[6] C. Fuglesang, M.G. de Herreros Miciano, Realistic sunshade system at L1 for global temperature control, Acta Astronaut. 186 (2021) 269–279, http://dx.doi.org/10.1016/j.actaastro.2021.04.035.
[7] O. Borgue, A.M. Hein, Transparent occulters: A nearly zero-radiation pressure sunshade to support climate change mitigation, Acta Astronaut. 203 (2023) 308–318, http://dx.doi.org/10.1016/j.actaastro.2022.12.006.
[8] J. Town, N. Pushparaj, C. Cappelletti, Preliminary structural system design for planetary sunshade, Aerospace 12 (9) (2025) 785, http://dx.doi.org/10.3390/aerospace12090785.
[9] C.L. Matonti, M. Coco, C. Cappelletti, B. Chesley, C. Fuglesang, G. Governale, N. Pushparaj, M. Romano, G. Tibert, L. Wilk, Roadmap Toward a Planetary Sunshade for Space-based Solar Geoengineering, Adv. Space Res. (2026) http://dx.doi.org/10.1016/j.asr.2026.04.007.
[10] M. Coco, C.L. Matonti, C. Cappelletti, B. Chesley, C. Fuglesang, G. Governale, N. Pushparaj, M. Romano, G. Tibert, L. Wilk, Planetary Sunshade for Solar Geoengineering: Preliminary Design of a Precursor System and Mission, Acta Astronaut. 235 (2025) 452–462, http://dx.doi.org/10.1016/j.actaastro.2025.05.031.
[11] M. Coco, C.L. Matonti, G. Governale, E. Ancona, R.Y. Kezerashvili, Performance of solar-sail materials at the photo-gravitational equilibrium point L1, Adv. Space Res. (2026) http://dx.doi.org/10.1016/j.asr.2026.06.036, URL https://www.sciencedirect.com/science/article/pii/S0273117726008094.
[12] T. Maheswaran, S. Fasoulas, Combining MBSE & MBE for Complex Space Mission Design: An Approach based on the System Analysis of the International Planetary Sunshade (IPSS) for Climate Mitigation, University of Stuttgard, 2024.
[13] B. Govindasamy, K. Caldeira, Geoengineering Earth's radiation balance to mitigate CO2-induced climate change, Geophys. Res. Lett. 27 (14) (2000) 2141–2144, http://dx.doi.org/10.1029/1999GL006086.
[14] R. Sun, D. Maessen, J. Guo, E. Gill, Enabling inter-satellite communication and ranging for small satellites, in: 9th Symposium on Small Satellites Systems and Services, Funchal, Portugal, vol. 31, 2010.
[15] S. Friedenthal, R. Griego, M. Sampson, INCOSE model based systems engineering (MBSE) initiative, in: INCOSE 2007 Symposium, vol. 11, sn, 2007.
[16] S.J. Kapurch, NASA Systems Engineering Handbook, Diane Publishing, 2010.
[17] E. Secretariat, System engineering general requirements, in: ECSS-E-ST-10C Rev. 1, ESA-ESTEC, Requirements & Standards Division Noordwijk, The Netherlands, 2017.
[18] D. Kaslow, G. Soremekun, H. Kim, S. Spangelo, Integrated model-based systems engineering (MBSE) applied to the simulation of a CubeSat mission, in: 2014 IEEE Aerospace Conference, 2014, pp. 1–14, http://dx.doi.org/10.1109/AERO.2014.6836317.

[19] D. Kaslow, L. Anderson, S. Asundi, B. Ayres, C. Iwata, B. Shiotani, R. Thompson, Developing a CubeSat model-based system engineering (MBSE) reference model - interim status, in: 2015 IEEE Aerospace Conference, 2015, pp. 1–16, http://dx.doi.org/10.1109/AERO.2015.7118965.

[20] J.N. Buitrago-Leiva, J.J. Mejía, J.F. Puerta-Ibarra, I.F. Acero-Niño, A.F. Guarnizo-Saavedra, J. Rodriguez-Ferreira, L. Rojas-Rodriguez, F.L. Hernández-Torres, C.E. Arango-Cotacio, J.E. Salazar-Morales, et al., Preliminary design of satellite systems through the integration of model-based system engineering and agile methodologies: application to the 3ColStar mission, Aerospace 11 (9) (2024) 758, http://dx.doi.org/10.3390/aerospace11090758.

[21] R.B. Buruso, S. Himmiche, T. Tejumola, Y. Alemayehu, B. Rose, Model-based systems engineering in space applications: A comprehensive literature review, Syst. Eng. n/a (n/a) (2026) e70051, http://dx.doi.org/10.1002/sys.70051.

[22] P. van Schalkwyk, S. Whiteley, M. Goldman, Digital twin capabilities periodic table, Digit. Twin Consort. (2022).

[23] D.L. Edwards, C. Semmel, M.A. Hovater, M. Nehls, P.A. Gray, W.S. Hubbs, G. Wertz, Solar sail material performance property response to space environmental effects, in: E.W. Taylor (Ed.), in: Photonics for Space Environments IX, vol. 5554, SPIE International Society for Optics and Photonics, 2004, pp. 80–91, http://dx.doi.org/10.1117/12.562809, URL.

[24] L. Herbeck, C. Sickinger, M. Eiden, M. Leipold, Solar sail hardware developments, in: European Conference on Spacecraft Structures, Materials and Mechanical Testing, Toulouse, 2002, pp. 1–10.

[25] S. Gong, M. Macdonald, Review on solar sail technology, Astrodynamics 3 (2) (2019) 93–125, http://dx.doi.org/10.1007/s42064-019-0038-x.

[26] S.P. Trofimov, M.Y. Ovchinnikov, Performance scalability of square solar sails, J. Spacecr. Rockets 55 (1) (2018) 241–244, http://dx.doi.org/10.2514/1.A33894.

[27] K. Wilkie, The NASA advanced composite solar sail system (ACS3) flight demonstration: A technology pathfinder for practical smallsat solar sailing, 2021, http://dx.doi.org/10.26077/px06-xg75.

[28] M. Berthet, J. Schalkwyk, O. Çelik, D. Sengupta, K. Fujino, A.M. Hein, L. Tenorio, J. Cardoso dos Santos, S.P. Worden, P.D. Mauskopf, Y. Miyazaki, I. Funaki, S. Tsuji, P. Fil, K. Suzuki, Space sails for achieving major space exploration goals: Historical review and future outlook, Prog. Aerosp. Sci. 150 (2024) 101047, http://dx.doi.org/10.1016/j.paerosci.2024.101047.

[29] M. Macdonald, G.W. Hughes, C.R. McInnes, A. Lyngvi, P. Falkner, A. Atzei, Solar polar orbiter: a solar sail technology reference study, J. Spacecr. Rockets 43 (5) (2006) 960–972, http://dx.doi.org/10.2514/1.16408.

[30] V. Lappas, B. Wie, Advanced satellite bus technology for near-term solar sail missions, in: AIAA/AAS Astrodynamics Specialist Conference and Exhibit, 2006, p. 6179, http://dx.doi.org/10.2514/6.2006-6179.

[31] G. Di Pietro, Planetary Sunshade for Solar Geoengineering: Attitude and Orbit Control for Solar-Sail Satellites (Master's thesis), Politecnico di Torino, 2026, URL https://webthesis.biblio.polito.it/id/eprint/40859.

[32] P.-Y. Shen, R.J. Caverly, Solar sail momentum management with mass translation and reflectivity devices using predictive control, Acta Astronaut. 241 (2026) 134–152, http://dx.doi.org/10.1016/j.actaastro.2025.12.042.

[33] A.A.C. Clyde Space, RW400 CubeSat Reaction Wheels, 2026, https://www.aac-clyde.space/what-we-do/space-products-components/adcs/rw400. (Accessed 09 June 2026).

[34] J. Orphee, B. Diedrich, B. Stiltner, C. Becker, A. Heaton, Solar sail attitude control system for the NASA near earth asteroid scout mission, in: International Symposium on Solar Sailing, (M17-5741) 2017.

[35] Y. Tsuda, O. Mori, R. Funase, H. Sawada, T. Yamamoto, T. Saiki, T. Endo, J. Kawaguchi, Flight status of IKAROS deep space solar sail demonstrator, Acta Astronaut. 69 (9–10) (2011) 833–840, http://dx.doi.org/10.1016/j.actaastro.2011.06.005.

[36] T. Theodorou, Three-Axis Attitude Control of Solar Sails Utilising Reflectivity Control Devices (Ph.D. thesis), University of Surrey, Guildford, United Kingdom, 2016, URL https://openresearch.surrey.ac.uk/esploro/outputs/doctoral/Three-axis-attitude-control-of-solar-sails/99513206202346.

[37] EnduroSat, CubeSat Modules and Satellite Platforms, 2026, https://www.endurosat.com/. (Accessed 09 June 2026).

[38] J. Wertz, W. Larson, Space Mission Analysis and Design, in: Space Mission Analysis and Design, (v. 8) Springer Netherlands, 1999.